INORGANIC CHEMISTRY FRONTIERS

RESEARCH ARTICLE

View Article Online
View Journal

Cite this: DOI: 10.1039/d5qi02415c

$ZnGa(SeO_3)_2F$: a UV transparent birefringent crystal explored in M(II)–IIIA–selenite–F systems

Tian-Tian He,[b,c] Chun-Li Hu,[b] Ya-Ping Gong,*[a,b] Jiang-Gao Mao [b,c] and Fang Kong *[b]

In this work, we present a targeted design strategy that combines Group IIIA metal cations and fluorine anions to simultaneously enhance the band gap and birefringence in selenite-based systems. Three new ultraviolet (UV) transparent selenite fluorides, $SrAl(SeO_3)F_3$ (**1**), $BaAl(SeO_3)F_3(H_2O)_{0.25}$ (**2**), and $ZnGa(SeO_3)_2F$ (**3**), were successfully synthesized under mild hydrothermal conditions. Remarkably, all three compounds exhibit wide band gaps as well as large birefringence. In particular, $ZnGa(SeO_3)_2F$ (**3**) demonstrates a pronounced birefringence value of 0.176 at 546 nm, representing the highest birefringence reported among all known selenites with a band gap above 5.0 eV. Theoretical investigations indicate that the strong optical anisotropy is predominantly attributed to the stereochemically active lone-pair electrons of Se(IV) cations. The $[Zn_2O_8]$ dimers and the infinite $[GaO_4F]_\infty$ chains in $ZnGa(SeO_3)_2F$ (**3**) crucially facilitate the optimal spatial arrangement of $[SeO_3]$ groups. This study expands the structural diversity of selenite fluorides and provides an effective pathway for designing high-performance birefringent crystals suitable for UV applications.

Received 27th November 2025,
Accepted 18th December 2025

DOI: 10.1039/d5qi02415c

rsc.li/frontiers-inorganic

Introduction

Birefringent crystals, as vital optical components, are indispensable in modulators, sensors, and isolators, finding extensive applications across commercial, industrial, and military sectors.[1–7] Although several established materials, including α-BaB_2O_4,[8] YVO_4,[9] $CaCO_3$,[10] and MgF_2,[11] have been commercialized, their performance in high-end optical systems is constrained by inherent limitations. These include the phase transition and facile deliquescence exhibited by α-BaB_2O_4. Additionally, there are challenges in growing sizable single crystals of YVO_4 and $CaCO_3$. MgF_2 has notably low birefringence, and YVO_4 has limited transparency for wavelengths below 400 nm.[12–14] Concurrently, the ongoing miniaturization of short-wavelength optical devices imposes an escalating demand for crystals that possess a wide band gap and large birefringence.[15] However, achieving this combination is fundamentally challenging due to the inherent trade-off between these two properties, rendering high-performance candidates exceedingly scarce.[16] Therefore, overcoming these material limitations and strategically balancing the band gap and birefringence constitute critical and urgent objectives in the pursuit of next-generation birefringent materials.[17–19]

The presence of stereochemically active lone-pair electrons in metal selenites gives rise to pronounced optical anisotropy, rendering these compounds suitable for birefringent applications. To date, numerous metal selenite crystals have been reported. These include compounds containing cations with stereochemically active lone pairs, such as $Pb_2(SeO_3)(SiF_6)$ (0.161@532 nm, 4.40 eV),[20] $Pb_2Bi(SeO_3)_2Cl_3$ (0.186@1064 nm, 3.45 eV),[21] and $Rb_2Bi_2(SeO_3)_3F_2$ (0.105@546 nm, 3.72 eV).[22] Others include d^0 transition metal ions characterized by their tendency toward second-order Jahn–Teller distortion, exemplified by $Gd_2F_2(OH_2)(MoO_3)_2(SeO_3)_2$ (0.143@1064 nm, 3.15 eV),[23] $Bi_4TiO_2F_4(SeO_3)_4$ (0.190@1064 nm, 3.58 eV),[24] and $Pb_2(V_2O_4F)(VO_2)(SeO_3)_3$ (0.105@1064 nm, 2.35 eV).[25] A further category involves d^{10} transition metals characterized by high polarizability and distortability, such as $Hg_2(SeO_3)(SO_4)$ (0.133@532 nm, 3.58 eV),[26] $Hg_3(SeO_3)_2(SO_4)$ (0.118@546 nm, 4.70 eV),[27] $Rb_2Hg_2(SeO_3)_3$ (0.055@546 nm, 3.60 eV),[28] $Pb_2Cd(SeO_3)_2Cl_2$ (0.093@1064 nm, 4.10 eV),[29] and $Pb_2Cd(SeO_3)_2Br_2$ (0.116@1064 nm, 3.90 eV).[29] However, a prevalent limitation among these compounds is their band gap (<5.0 eV), which significantly restricts their application in the UV spectral region. To address this issue, researchers have introduced ions conducive to widening the band gap within the selenite system, such as alkali and alkaline earth metals. This strategy has successfully yielded a series of wide-band gap selenites,

[a]Shandong Sport University, Jinan 250102, P. R. China. E-mail: gongyaping@sdpei.edu.cn
[b]State Key Laboratory of Functional Crystals and Devices, Fujian Institute of Research on the Structure of Matter, Chinese Academy of Sciences, Fuzhou 350002, P. R. China. E-mail: kongfang@fjirsm.ac.cn
[c]School of Physical Science and Technology, ShanghaiTech University, Shanghai, 201210, P. R. China

including $Na_8(SeO_3)(SO_4)_3$ (5.69 eV, 0.038@1064 nm),[30] $Na_2(H_2SeO_3)(SO_4)$ (5.04 eV, 0.082@1064 nm),[30] and $NaGa_3(HSeO_3)_6(SeO_3)_2$ (5.20 eV, 0.003@1064 nm).[16] Nevertheless, although their band gaps exceed 5.0 eV, the birefringence values of these compounds exhibit a notable decrease, mainly due to the limited contribution of these cations to the anisotropy of polarizability.

Based on extensive literature surveys, fluoride ions (F^-), which belong to Group VIIA, possess high electronegativity and strong UV transparency.[31–33] The introduction of fluoride ions has been established as one effective strategy for band gap enlargement, as demonstrated by $A(GaF_2)_3(SeO_3)_2$ (A = K and NH_4),[34] demonstrating wide band gaps of 5.62 and 5.77 eV, respectively. Meanwhile, the introduction of Group IIIA metals, such as Al^{3+} and Ga^{3+}, does not compromise the band gap, because these metals lack d–d electronic transitions, which could narrow the band gap.[35–38] So far, fluorinated Group IIIA selenites have been predominantly reported in alkali metal and Pb^{2+}-based systems, whereas fluorinated Group IIIA selenites incorporating divalent alkaline earth or transition metal cations remain unexplored. Similar to alkali metals, alkaline earth cations possess no d–d and f–f electronic transitions and exhibit strong ionic character, which effectively widens the band gap of their corresponding compounds.[39,40] Furthermore, d^{10} transition metal cations (*e.g.*, Zn^{2+} and Hg^{2+}), with their high polarization and deformability, are promising for producing materials with large optical birefringence.[41,42] With the aim of developing materials that combine wide band gaps and pronounced birefringence, our research targeted gallium/aluminum selenite fluoride systems. Our work in the M^{II}–Ga^{III}/Al^{III}–Se^{IV}–O–F systems culminated in the discovery of three novel selenite birefringent materials: $SrAl(SeO_3)F_3$ (**1**), $BaAl(SeO_3)F_3(H_2O)_{0.25}$ (**2**), and $ZnGa(SeO_3)_2F$ (**3**). All three synthesized compounds feature band gaps greater than 5.0 eV. $SrAl(SeO_3)F_3$ and $BaAl(SeO_3)F_3(H_2O)_{0.25}$ display birefringence values of 0.059 and 0.082 at 546 nm, respectively, whereas $ZnGa(SeO_3)_2F$ exhibits a substantially higher birefringence of 0.176 at the same wavelength. In this work, we present an in-depth analysis of their synthesis procedures, crystal structures, thermal stabilities, and optical properties.

Experimental section

Reagents

SeO_2 (Adamas-beta, 99.99%), Al_2O_3 (Aladdin, 99.9%), Ga_2O_3 (Aladdin, 99.9%), $ZnF_2{\cdot}4H_2O$ (Adamas, 98%+), SrF_2 (Adamas, 99.9%), BaF_2 (Adamas, 99.9%), and HF (40%, AR) were obtained from commercial sources and used without further purification.

Syntheses

The three compounds were synthesized *via* a mild hydrothermal reaction. The chemical ratios for each compound are as follows: for $SrAl(SeO_3)F_3$ (**1**), the reactants included SeO_2 (0.222 mg, 2 mmol), Al_2O_3 (0.102 mg, 1 mmol), SrF_2 (0.126 mg, 1 mmol), hydrofluoric acid (0.25 mL) and 2.5 mL of deionized water. For $BaAl(SeO_3)F_3{\cdot}(H_2O)_{0.25}$ (**2**), the reactants included SeO_2 (0.222 mg, 2 mmol), Al_2O_3 (0.102 mg, 1 mmol), BaF_2 (0.175 mg, 1 mmol), hydrofluoric acid (0.25 mL) and 2.5 mL of deionized water. For $ZnGa(SeO_3)_2F$ (**3**), the reactants included SeO_2 (0.222 mg, 2 mmol), Ga_2O_3 (0.187 mg, 1 mmol), $ZnF_2{\cdot}4H_2O$ (0.175 mg, 1 mmol), hydrofluoric acid (0.25 mL) and 2.5 mL of deionized water. These mixtures were then sealed in a Teflon liner with a volume of 23 mL and heated at 220 °C for a duration of 4 days. Following this, they were cooled to room temperature at a rate of 3 °C h^{-1}. The resulting products were isolated through vacuum filtration, washed with alcohol, and dried at ambient temperature. Elemental distribution maps provided definitive evidence for the chemical composition of each compound (Fig. 1). As shown in Fig. S2, their purity was verified through X-ray diffraction (XRD) studies.

Single-crystal structure determination

Single-crystal XRD data of $SrAl(SeO_3)F_3$, $BaAl(SeO_3)F_3(H_2O)_{0.25}$, and $ZnGa(SeO_3)_2F$ were collected using a Rigaku Oxford Diffraction SuperNova CCD diffractometer on a 293 K (Mo) X-ray source (λ = 0.71073 Å). Data reduction and cell refinement were executed using CrysAlisPro. The structure was elucidated through direct methods and subsequently refined *via* full-matrix least squares fitting on F^2, utilizing the OLEX 2-1.5 and SHELXL-2017 crystallographic software packages.[43,44] All atoms underwent refinement with anisotropic thermal parameters. The structural data were further validated using PLATON, revealing no evidence of higher symmetry.[45,46] The detailed crystallographic data of the three structures are listed in Table 1, and some selected atomic bond lengths and bond valences are reported in Table S2.

Powder X-ray diffraction

Powder XRD patterns of the three compounds were collected on a MiniFlex 600 powder X-ray diffractometer using Cu Kα radiation (λ = 1.54186 Å) at room temperature in the angular range of 2θ = 10–70° with a scan step size of 0.02°.

Energy-dispersive X-ray spectroscopy

Elemental analysis was carried out with the aid of a field-emission scanning electron microscope (FESEM, JSM6700F)

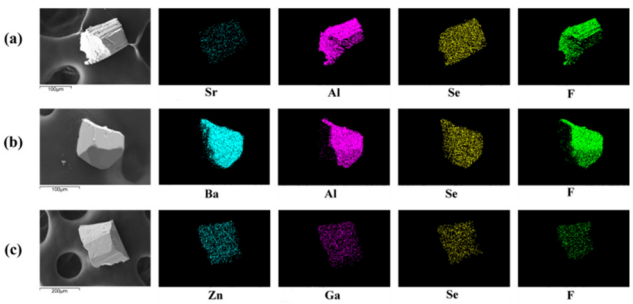

Fig. 1 SEM images of $SrAl(SeO_3)F_3$ (a), $BaAl(SeO_3)F_3(H_2O)_{0.25}$ (b), and $ZnGa(SeO_3)_2F$ (c) and their elemental distribution maps.

Table 1 Crystal data and structure refinement for $SrAl(SeO_3)F_3$ (**1**), $BaAl(SeO_3)F_3(H_2O)_{0.25}$ (**2**) and $ZnGa(SeO_3)_2F$ (**3**)

Empirical formula	$SrAl(SeO_3)F_3$	$BaAl(SeO_3)F_3(H_2O)_{0.25}$	$ZnGa(SeO_3)_2F$
Formula weight	298.56	352.78	408.01
Temperature (K)	293(2)	293(2)	293(2)
Crystal system	Hexagonal	Tetragonal	Monoclinic
Space group	$P6_3/m$	$P4/n$	$P2_1/c$
a (Å)	13.2436(8)	14.5731(4)	7.3482(5)
b (Å)	13.2436(8)	14.5731(4)	12.3498(8)
c (Å)	5.1816(4)	5.0773(3)	7.7071(4)
α (°)	90	90	90
β (°)	90	90	121.237(5)
γ (°)	120	90	90
Volume (Å^3)	787.06(11)	1078.29(9)	598.02(7)
Z	6	8	4
D_c (g cm^{-3})	3.779	4.346	4.532
μ (mm^{-1})	17.374	14.281	20.686
λ (Mo Kα) (Å)	0.71073	0.71073	0.71073
GOF on F^2	1.106	1.165	1.245
R_1, wR_2 $[I > 2\sigma(I)]^a$	0.0238, 0.0554	0.0161, 0.0327	0.0407, 0.0928
R_1, wR_2 (all data)^a	0.0255, 0.0567	0.0203, 0.0343	0.0445, 0.0942
CCDC	2500271	2500272	2500273

$^a R_1 = \sum||F_o| - |F_o||/\sum|F_o|$, $wR_2 = [w(F_o^2 - F_c^2)^2]/[wF_o^4]^{1/2}R_1$.

equipped with an energy dispersive X-ray spectroscope (EDS, Oxford INCA).

Spectroscopic measurements

Infrared (IR) spectra were analyzed utilizing a Magna 750 FT-IR spectrometer, employing air as the background. The analysis was conducted within the range of 4000–400 cm^{-1} and achieved a resolution of 2 cm^{-1} at room temperature. UV-vis-NIR spectra were acquired within the 2000–200 nm range using a PerkinElmer Lambda 900 spectrophotometer, with $BaSO_4$ serving as the reference. The reflection spectra were subsequently transformed into absorption spectra through the application of the Kubelka–Munk function. Absorption data were derived from the diffuse reflection data utilizing the Kubelka–Munk function: $\alpha/S = (1 - R)^2/2R$, where α and S denote the absorption coefficient and scattering coefficient, respectively. The band gap value can be determined by extrapolating the absorption edge to the baseline in the α/S *versus* energy graph.[47]

Thermal analysis

Thermogravimetric analyses (TGA) were carried out using the Netzsch STA 449F3 installation. About 3.0–5.0 mg of samples were placed in alumina crucibles and heated from 20 to 1000 °C at a rate of 15 K min^{-1} under a N_2 atmosphere.

Results and discussion

Crystal structure descriptions

$SrAl(SeO_3)F_3$ and $BaAl(SeO_3)F_3(H_2O)_{0.25}$ have been found to crystallize in the centrosymmetric space groups $P6_3/m$ (no. 176) and $P4/n$ (no. 85), respectively. The asymmetric unit of $SrAl(SeO_3)F_3$ consists of one Sr, one Se, one Al, two F, and two O atoms. Al exhibits an octahedral geometry coordinated by three O and three F atoms, forming $[AlF_3O_3]$ units, where the Al–O bond lengths span 1.851(9) to 1.914(8) Å. Se1 coordinates with three O atoms, forming an asymmetric trigonal pyramidal structure with Se–O bond lengths of 1.671(6) to 1.690(1) Å. Valence calculations suggest Al and Se oxidation states of +3 and +4. The asymmetric unit of $BaAl(SeO_3)F_3(H_2O)_{0.25}$ contains one Ba, one Al, one Se, one H, three F, and four O. It was observed that Al in $BaAl(SeO_3)F_3(H_2O)_{0.25}$ adopted a six-coordinate $[AlF_3O_3]$ octahedral geometry with Al–O bond lengths ranging from 1.865(2) to 1.950(5) Å. This finding is analogous to that of $SrAl(SeO_3)F_3$. Se also coordinates with three O atoms, forming an asymmetric trigonal pyramidal structure with Se–O bond lengths ranging from 1.681(6) to 1.697(2) Å. Valence calculations suggest oxidation states of +3 for Al and +4 for Se, as illustrated in Table S2.[48,49]

$SrAl(SeO_3)F_3$ and $BaAl(SeO_3)F_3(H_2O)_{0.25}$ exhibit structural characteristics that are analogous to each other, as shown in Fig. 2. $[AlF_3O_3]$ octahedra and $[SeO_3]$ trigonal pyramids establish connections *via* shared oxygen atoms, thereby forming

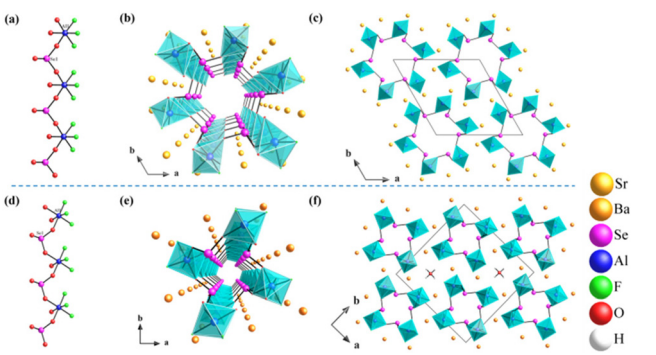

Fig. 2 Structural features of $SrAl(SeO_3)F_3$ and $BaAl(SeO_3)F_3(H_2O)_{0.25}$: 1D $[AlSeF_3O_4]_\infty$ chains along the c axis (a and d); 1D porous frameworks with hexagonal (Sr) or tetragonal (Ba) pores (b and e); and 3D structures illustrating cation arrangements within the pores (c and f).

one-dimensional (1D) $[AlSeF_3O_4]_\infty$ chains along the *c* axis (Fig. 2a and d).

These chains are interconnected by oxygen atoms at the extremities of $[SeO_3]$ trigonal pyramids, thereby establishing a 1D porous framework along the *c*-axis. In $SrAl(SeO_3)F_3$, this process results in the formation of hexagonal pores, with Sr^{2+} cations occupying the interstitial spaces (Fig. 2c). $BaAl(SeO_3)F_3(H_2O)_{0.25}$ features tetragonal pores as well, with Ba^{2+} cations occupying the interstices between these pores (Fig. 2e).

$ZnGa(SeO_3)_2F$ crystallizes in the monoclinic space group $P2_1/c$. Its asymmetric unit comprises 11 atoms: one Zn, one Ga, two Se, one F, and six O atoms. The Ga atom exhibits an octahedral coordination environment, bonded to four oxygen and two fluorine atoms. The Ga–O bond distances vary from 1.901(9) Å to 1.967(0) Å, while Ga–F bonds range between 1.951(2) Å and 1.953(8) Å. Each Se atom is coordinated by three oxygen atoms, forming a $[SeO_3]$ trigonal pyramidal unit, with the Se–O bond lengths spanning 1.669(4) Å to 1.751(4) Å. Zinc is coordinated by oxygen atoms with Zn–O distances in the range of 1.960(0) Å to 2.137(4) Å. Bond valence sum calculations yield values of 1.98, 3.25, 3.95, and 3.92 for Zn, Ga, Se (1), and Se(2), respectively, consistent with oxidation states of +2 for Zn, +3 for Ga, and +4 for Se (Table S2).[48,49] $ZnGa(SeO_3)_2F$ has a novel 3D network structure. As illustrated in Fig. 3, the six-coordinated $[GaO_4F_2]$ octahedra share F atoms along the *c*-axis, forming $[GaO_4F]_\infty$ 1D chains (Fig. 3a). These chains are interconnected *via* $[Se(1)O_3]$ units to create a 2D layer parallel to the *ac* plane (Fig. 3c). Two $[ZnO_5]$ polyhedra form a $[Zn_2O_8]$ dimer (Fig. 3b). This dimer shares O atoms with $[Se(1)O_3]$ and $[Se(2)O_3]$ units, generating a separate 1D chain extending along the *a*-axis (Fig. 3d). The final 3D framework arises from the interconnection of the 2D layers by these 1D chains composed of $[Zn_2O_8]$ dimers and $[SeO_3]$ units (Fig. 3e).

Thermal analyses

Thermogravimetric analyses of compounds **1–3** were conducted under a nitrogen atmosphere over the temperature range of 20 to 1000 °C. $SrAl(SeO_3)F_3$, $BaAl(SeO_3)F_3(H_2O)_{0.25}$ and $ZnGa(SeO_3)_2F$ demonstrate thermal stability up to 508 °C, 430 °C, and 396 °C, respectively, with mass losses of 37.9%, 32.1%, and 58.1% occurring over the temperature ranges of 508–800 °C, 430–800 °C and 396–900 °C, in the same order. For $SrAl(SeO_3)F_3$, the subsequent mass loss is attributed to the evolution of one SeO_2, while for $BaAl(SeO_3)F_3(H_2O)_{0.25}$, it involves the release of the same species along with water. For $ZnGa(SeO_3)_2F$, the mass loss in the 396–900 °C range corresponds to the volatilization of one equivalent of SeO_2 and half an equivalent of F_2 (Fig. S3).

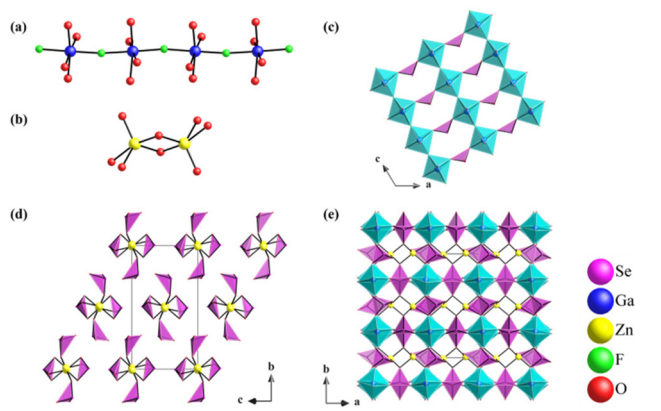

Fig. 3 The 1D $[GaO_4F]_\infty$ chain (a), $[Zn_2O_8]$ dimers (b), 2D layer constructed from the chains and $Se(1)O_3$ units (c), 1D chain based on $[Zn_2O_8]$ dimers and $[SeO_3]$ units (d), and the overall 3D framework of $ZnGa(SeO_3)_2F$ (e).

IR and UV-vis-NIR spectra

IR spectra of compounds **1–3** were obtained in the range of 400–4000 cm^{-1}. All three compounds show strong absorption in the range of 563–609 cm^{-1}, which is attributed to the absorption of fluorine ions. The prominent absorption peaks at 708–911 cm^{-1} correspond to the stretching and bending vibrations of Se–O bonds.[50] Additionally, the peaks at 433–519 cm^{-1} and 432–492 cm^{-1} correspond to the stretching vibrations of Al–O and Ga–O bonds, respectively. In particular, the distinct absorption peaks at 3180 cm^{-1} and 1601 cm^{-1} are attributed to O–H vibrational modes.[51] All vibrational assignments are well supported by the existing literature (Fig. S4).

As shown in Fig. 4, the UV-vis-NIR diffuse reflectance spectra indicate minima in reflectance for $SrAl(SeO_3)F_3$ and $BaAl(SeO_3)F_3(H_2O)_{0.25}$ at about 200 nm and for $ZnGa(SeO_3)_2F$ at 213 nm. The optical band gaps of the three compounds are 5.41 eV, 5.50 eV, and 5.01 eV, respectively. These band gap values exceed those of most selenite fluorides reported previously, such as $RbGa_3F_6(SeO_3)_2$ (3.57 eV),[52] $CsGa_3F_6(SeO_3)$ (3.65 eV),[52] $LiBa_3Bi_6(SeO_3)_7F_{11}$ (3.80 eV),[53] and $Bi_3(SeO_3)_3(Se_2O_5)F$ (3.80 eV),[54] and are comparable to the largest band gaps for inorganic selenites, for instance, $NH_4(GaF_2)_3(SeO_3)_2$ (5.77 eV)[34] and $K_4(GaF_2)_3(SeO_3)_2$ (5.62 eV),[34] which underscores their unique optical properties.

Theoretical calculations

Density functional theory (DFT) calculations were performed to explore the electronic structures and linear optical properties of compounds **1–3**, aiming to elucidate their structure–property correlations.[55] The computed band gap values were 5.07, 5.31, and 4.35 eV, respectively (Fig. S5). Consistent with the known tendency of the GGA-PBE functional (where GGA stands for generalized gradient approximation and PBE for Perdew–Burke–Ernzerhof) to underestimate band gaps due to a lower conduction band energy prediction, the calculated values are smaller than the experimental measurements. To compensate for this discrepancy and enhance the accuracy of the optical property simulations, scissor operators of 0.34, 0.19, and 0.66 eV were introduced for $SrAl(SeO_3)F_3$, $BaAl(SeO_3)F_3(H_2O)_{0.25}$ and $ZnGa(SeO_3)_2F$, respectively.

To further elucidate the electronic structures, total and partial density of states (DOS) calculations were performed for the three compounds, as depicted in Fig. S6. Examination of the states near the Fermi level reveals the atomic orbitals con-

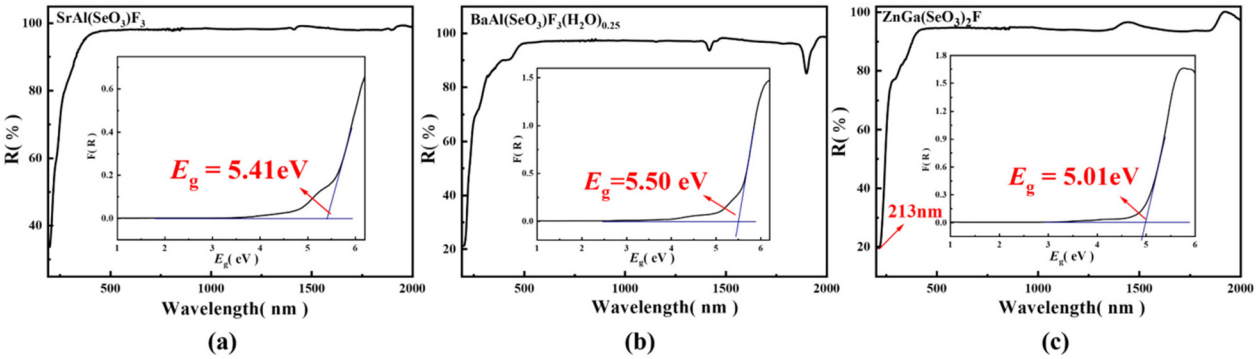

Fig. 4 UV-vis-NIR diffuse-reflectance spectra of $SrAl(SeO_3)F_3$ (a), $BaAl(SeO_3)F_3(H_2O)_{0.25}$ (b), and $ZnGa(SeO_3)_2F$ (c).

tributing to the band edges. For $SrAl(SeO_3)F_3$, the valence band maximum is primarily derived from O-2p and Se-4s4p orbitals, and the conduction band minimum mainly arises from Se-4p orbitals. For $BaAl(SeO_3)F_3(H_2O)_{0.25}$, the valence band edge predominantly consists of O-2p states, with the conduction band bottom dominated by Se-4p orbitals. In $ZnGa(SeO_3)_2F$, the valence band maximum features significant contributions from O-2p and Se-4s4p states, while the conduction band minimum is chiefly composed of Se-4p and Zn-4s orbitals. These results indicate that the band gaps of $SrAl(SeO_3)F_3$ and $BaAl(SeO_3)F_3(H_2O)_{0.25}$ are determined by Se and O atoms, and the band gap of $ZnGa(SeO_3)_2F$ is governed by Se, O and Zn atoms.

Birefringence

The linear optical properties of the three compounds were analyzed through the complex dielectric function $\varepsilon(\omega) = \varepsilon_1(\omega) + i\varepsilon_2(\omega)$, revealing distinct refractive indices along the 100, 010, and 001 crystallographic directions. Compounds **1–3** exhibit the following refractive index sequences: $n_{001} > n_{010} > n_{100}$ for $SrAl(SeO_3)F_3$, $n_{010} > n_{100} > n_{001}$ for $BaAl(SeO_3)F_3(H_2O)_{0.25}$, and $n_{100} > n_{010} > n_{001}$ for $ZnGa(SeO_3)_2F$ (Fig. 5). The computed birefringence values at 546 nm are 0.059 and 0.082 for $SrAl(SeO_3)F_3$ and $BaAl(SeO_3)F_3(H_2O)_{0.25}$, respectively, decreasing slightly at 1064 nm to 0.053 and 0.075. In contrast, $ZnGa(SeO_3)_2F$ exhibits significantly enhanced birefringence, reaching 0.176 at 546 nm and 0.163 at 1064 nm. It is noteworthy that the birefringence of $ZnGa(SeO_3)_2F$ exceeds those of all reported selenites with wide band gaps (>5.0 eV) to date, as presented in Fig. 6.[56] The electron density difference map of $ZnGa(SeO_3)_2F$ reveals that the lone pair electrons of Se(IV) exhibit pronounced stereochemical activity (Fig. S7). It can also be observed that the lone pair electrons on the Se atom in the [Se(IV)O_3] group adopt a linear alignment. This structural feature contributes

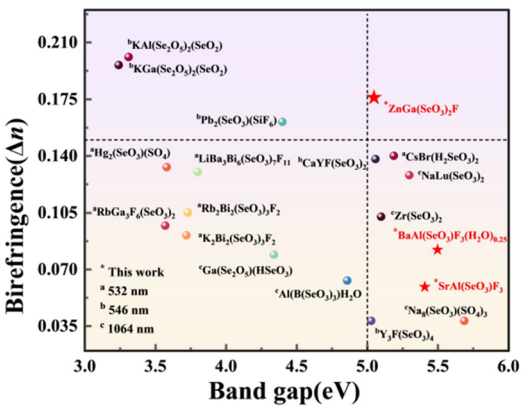

Fig. 6 Reported birefringence and band gaps of selenites.

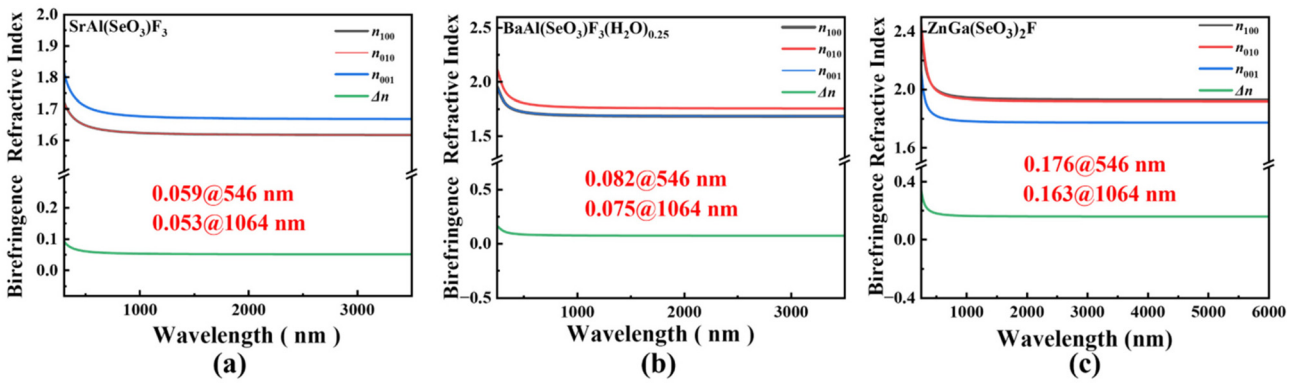

Fig. 5 Calculated refractive indices and birefringence values of $SrAl(SeO_3)F_3$ (a), $BaAl(SeO_3)F_3(H_2O)_{0.25}$ (b), and $ZnGa(SeO_3)_2F$ (c).

significantly to the large birefringence of $ZnGa(SeO_3)_2F$. In comparison with $BaAl(SeO_3)F_3(H_2O)_{0.25}$ and $SrAl(SeO_3)F_3$, the two $[ZnO_5]$ polyhedra forming a $[Zn_2O_8]$ dimer and $[GaO_4F]_\infty$ chains in $ZnGa(SeO_3)_2F$ play an essential role in modulating the arrangement of the lone pair-containing $[SeO_3]$ polyhedra.

Conclusions

In summary, three novel selenite fluoride crystals, $SrAl(SeO_3)F_3$ (**1**), $BaAl(SeO_3)F_3(H_2O)_{0.25}$ (**2**) and $ZnGa(SeO_3)_2F$ (**3**), have been successfully synthesized *via* mild hydrothermal methods. These compounds exhibit unique structural frameworks, including a 1D porous framework in $SrAl(SeO_3)F_3$ and $BaAl(SeO_3)F_3(H_2O)_{0.25}$ and a 3D network in $ZnGa(SeO_3)_2F$ constructed from $[GaO_4F]_\infty$ chains, $[Zn_2O_8]$ dimers, and $[SeO_3]$ units. Remarkably, all three compounds achieve an excellent balance between a wide band gap and large birefringence. Among them, $ZnGa(SeO_3)_2F$ stands out with an ultra-large birefringence (0.176 at 546 nm) and a wide band gap (5.01 eV). Notably, its birefringence is the largest among all reported selenites with a band gap exceeding 5.0 eV. Theoretical calculations reveal that the large birefringence primarily originates from the stereochemically active lone pairs of Se(IV) in the $[SeO_3]$ groups, as well as the specific arrangement modulated by $[Zn_2O_8]$ dimers and $[GaO_4F]_\infty$ chains in $ZnGa(SeO_3)_2F$. This work not only enriches the family of selenite-based optical crystals but also demonstrates the effectiveness of combining fluorine and Group IIIA metal cations in designing new birefringent materials with both wide band gaps and large optical anisotropy.

Author contributions

Tian-Tian He: validation and writing – original draft; Chun-Li Hu: formal analysis; Ya-Ping Gong: investigation, validation and funding acquisition; Jiang-Gao Mao: supervision and funding acquisition; Fang Kong: conceptualization, supervision, writing – review and editing and funding acquisition.

Conflicts of interest

There are no conflicts to declare.

Data availability

The data that support the findings of this study are available in the supplementary information (SI). Supplementary information: computational method, important bond distances, bond valences, as-grown crystals, powder XRD, IR spectra, TGA results, band structures, total and partial density of states, and electron density difference map. See DOI: **https://doi.org/10.1039/d5qi02415c**.

CCDC 2500271–2500273 contain the supplementary crystallographic data for this paper.[57a–c]

Acknowledgements

This work was supported by the National Natural Science Foundation of China (Grant No. 22475215), the Natural Science Foundation of Fujian Province (Grant No. 2024J010039 and 2023j01216), the Self-Deployed Key Project of State Key Laboratory of Functional Crystals and Devices (GNJT-2025-ZD01) and the Shandong Provincial Natural Science Foundation (ZR2024QB208).

References

1 P. F. Chen, C. L. Hu, M. Z. Zhang and J. G. Mao, *β*-$LaTeBO_5$ and $RETeBO_5$ (RE = Y, Gd, Tb): explorations of new optical materials in the RE(III)–Te(IV)–B–O system, *Inorg. Chem. Front.*, 2025, **12**, 2638–2647.

2 C. Jin, Y. Li, C. A. Chen, J. Lee, C. Ko, S. Lee and K. M. Ok, Sulfonated Module Aggregation for Ultrahigh Birefringence in Aqueous-Processable Crystals, *J. Am. Chem. Soc.*, 2025, **147**, 39964–39973.

3 H. Li, H. Tian, P. Gong, T. Wang, H. Liu, B. Li, Q. Wu and M. Xia, A Band-Orientation Co-Anchoring Strategy for the Design of a High-Performance Mid-Infrared Nonlinear Optical Crystal, *Angew. Chem., Int. Ed.*, 2025, e202518549, DOI: **10.1002/anie.202518549**.

4 C. Shen, H. Zhou, C. Hu, Z. Yang, F. Zhang and S. Pan, $CN_4H_7B_3O_3F_2(OH)_2$: short-wave UV hydroxyfluorooxyborate crystals with large birefringence, *Chem. Commun.*, 2025, **61**, 16997.

5 R. L. Tang, W. Yue, Y. L. Lv, B. W. Miao, W. Liu and S. P. Guo, Significant enhancement in the birefringence of metal phosphite halides via the introduction of π-conjugated cations, *Chem. Sci.*, 2025, **16**, 22021–22028.

6 M. Z. Zhang, Y. Zhao, C. L. Hu and J. G. Mao, $BaSbBS_4$: a record-high-performance birefringent crystal identified by a target-driven closed-loop strategy, *Chem. Sci.*, 2025, **16**, 12577–12586.

7 X. T. Zhang, X. X. Jiang, H. Gao, K. N. Duanmu, C. Wu, Z. S. Lin, Z. P. Huang, M. G. Humphrey and C. Zhang, Breaking the Deep-UV Transparency/Optical Nonlinearity Trade-Off: Three-Parameter Optimization in Oxyfluorides by Tailoring d^0-Metal Incorporation, *Angew. Chem., Int. Ed.*, 2025, **64**, e202513438.

8 Z. Guoqing, X. Jun, C. Xingda, Z. Heyu, W. Siting, X. Ke, D. Peizhen and G. Fuxi, Growth and spectrum of a novel birefringent *α*-BaB_2O_4 crystal, *J. Cryst. Growth*, 1998, **191**, 517–519.

9 H. Luo, T. Tkaczyk, R. Sampson, E. Dereniak, H. Luo, T. Tkaczyk, R. Sampson and E. Dereniak, Birefringence of yttrium vanadate single crystals in the middle wave-

length infrared - art. no. 61190J, *Proc. SPIE*, 2006, **6119**, 136–142.
10 G. Ghosh, Dispersion-equation coefficients for the refractive index and birefringence of calcite and quartz crystals, *Opt. Commun.*, 1999, **163**, 95–102.
11 M. J. Dodge, Refractive properties of magnesium fluoride, *Appl. Opt.*, 1984, **23**, 1980–1985.
12 Q. Wu, T. Wang, J. Zhou, P. Gong, H. Li, H. Tian and M. Xia, Nonlinear Optical Series $A(VO_2)_3(SeO_3)_2$ (A = NH^{4+}, K^+, and H_3O^+) with Large Birefringence Derived from High-Anisotropic VO6 Octahedra and SeO3 Pyramids, *Inorg. Chem.*, 2025, **64**, 13549–13556.
13 J. Zhou, Q. Wu, A. Ji, Z. Jia and M. Xia, Recent progress in nonlinear optical molybdenum/tungsten tellurites: Structures, crystal growth and characterizations, *Coord. Chem. Rev.*, 2025, **524**, 216332.
14 X. Meng, H. Tian, Q. Wu and M. Xia, Nonlinear optical cyanurate crystals, *J. Cryst. Growth*, 2024, **648**, 127930.
15 S. Wang, Y. Zhang, Y. Yan, X. Dong, L. Cao, L. Huang and G. Zou, From $(C_{12}H_9N_2)_2TeBr_6{\cdot}2H_2O$ to $(C_{12}H_9N_2)_2TeBr_6$: Dehydration-Driven Crystal Reorganization for Birefringence Optimization, *Inorg. Chem.*, 2025, **64**, 20490–20497.
16 P. F. Li, Y. P. Gong, C. L. Hu, B. Zhang, J. G. Mao and F. Kong, Four UV Transparent Linear and Nonlinear Optical Materials Explored from Pure Selenite Compounds, *Adv. Opt. Mater.*, 2024, **12**, 2301426.
17 Y. Shen, J. Xiong, M. Wu, M. Li, Y. Zhou and Y. Zhang, Enhancing Birefringence via a Planar-Conformation-Locking Strategy, *Laser Photonics Rev.*, 2025, e01545, DOI: 10.1002/lpor.202501545.
18 Z. Sun, B. Wu, Z. Yu, Q. Ding, Y. Wang, M. Zhong, S. Zhao and J. Luo, Realizing large birefringence via S-substitution and anisotropic arrangement optimization, *Inorg. Chem. Front.*, 2025, DOI: 10.1039/D5QI01600B.
19 Y. Li, X. Song, B. Chen, Y. Song, W. Huang, J. Luo and S. Zhao, A transparent crystal with giant birefringence arising from π-electron anisotropy, *Mater. Today*, 2025, **87**, 29–35.
20 P. F. Li, C. L. Hu, J. G. Mao and F. Kong, $Pb_2(SeO_3)(SiF_6)$: the first selenite fluorosilicate with a wide bandgap and large birefringence achieved through perfluorinated group modification, *Chem. Sci.*, 2024, **15**, 7104–7110.
21 Y. J. Jia, X. Zhang, Y. G. Chen, X. Jiang, J. N. Song, Z. Lin and X. M. Zhang, $PbBi(SeO_3)_2F$ and $Pb_2Bi(SeO_3)_2Cl_3$: Coexistence of Three Kinds of Stereochemically Active Lone-Pair Cations Exhibiting Excellent Nonlinear Optical Properties, *Inorg. Chem.*, 2022, **61**, 15368–15376.
22 S. Shi, C. Lin, G. Yang, L. Cao, B. Li, T. Yan, M. Luo and N. Ye, $A_2Bi_2(SeO_3)_3F_2$ (A = K and Rb): Excellent Mid-Infrared Nonlinear Optical Materials with Both Strong SHG Responses and Large Band Gaps, *Chem. Mater.*, 2020, **32**, 7958–7964.
23 Y. X. Ma, P. F. Li, C. L. Hu, J. G. Mao and F. Kong, $Ln_2F_2(OH_2)(MoO_3)_2(SeO_3)_2$: Promising Multifunctional Nonlinear Optical Materials Created by Partial Fluorination Strategy under Corrosion Resistant Supercritical Reactions, *Adv. Sci.*, 2023, **10**, e2304463.
24 Y. P. Gong, C. L. Hu, F. Kong and J. G. Mao, Exploration of New Birefringent Crystals in Bismuth d0 Transition Metal Selenites, *Chem. – Eur. J.*, 2019, **25**, 3685–3694.
25 L. Lin, X. Jiang, C. Wu, Z. Lin, Z. Huang, M. G. Humphrey and C. Zhang, First chiral fluorinated lead vanadate selenite $Pb_2(V_2O_4F)(VO_2)(SeO_3)_3$ with five asymmetric motifs and large optical properties, *Dalton Trans.*, 2021, **50**, 7238–7245.
26 P. F. Li, C. L. Hu, F. Kong and J. G. Mao, $Hg_2(SeO_3)(SO_4)$: the first sulfate selenite with large birefringence explored from d10 transition metal compounds, *Mater. Chem. Front.*, 2022, **6**, 3567–3576.
27 J. Ren, Y. Chen, L. Ren, Y. Zhou, X. Dong, D. Gao, L. Huang, L. Cao and N. Ye, $Hg_3(SeO_3)_2(SO_4)$: A UV Nonlinear Optical Mercury Selenite Sulfate Constructed by Neat $[Hg_6O_8(SeO_3)_4]_\infty$ Layers and SO_4 Tetrahedra, *Inorg. Chem.*, 2023, **62**, 9130–9138.
28 J. Ren, H. Cui, L. Cheng, Y. Zhou, X. Dong, D. Gao, L. Huang, L. Cao and N. Ye, $A_2Hg_x(SeO_3)_y$ (A = K, Rb, Cs): Three Alkali Metal Mercury Selenites Featuring Unique 1D $[HgO_m(SeO_3)_n]_\infty$ Chains, *Inorg. Chem.*, 2023, **62**, 21173–21180.
29 Y. P. Gong, C. L. Hu, Y. X. Ma, J. G. Mao and F. Kong, $Pb_2Cd(SeO_3)_2X_2$ (X = Cl and Br): two halogenated selenites with phase matchable second harmonic generation, *Inorg. Chem. Front.*, 2019, **6**, 3133–3139.
30 X. W. Zhang, Z. X. Wang, C. L. Hu, Y. F. Li, J. G. Mao and F. Kong, UV-Transparent SHG Material Explored in an Alkali Metal Sulfate Selenite System, *Inorg. Chem.*, 2024, **63**, 6067–6074.
31 H. Qiu, F. Li, C. Jin, Z. Yang, J. Li, S. Pan and M. Mutailipu, Fluorination Strategy Towards Symmetry Breaking of Boron-centered Tetrahedron for Poly-fluorinated Optical Crystals, *Angew. Chem., Int. Ed.*, 2024, **63**, e202316194.
32 Y. Hu, X. Jiang, T. Wu, Y. Xue, C. Wu, Z. Huang, Z. Lin, J. Xu, M. G. Humphrey and C. Zhang, Wide bandgaps and strong SHG responses of hetero-oxyfluorides by dual-fluorination-directed bandgap engineering, *Chem. Sci.*, 2022, **13**, 10260–10266.
33 M. Yan, R. L. Tang, W. D. Yao, W. Liu and S. P. Guo, Exploring a new short-wavelength nonlinear optical fluoride material featuring unprecedented polar cis-$[Zr_6F_{34}]^{10-}$ clusters, *Chem. Sci.*, 2024, **15**, 2883–2888.
34 G. Park and K. M. Ok, Hexagonal tungsten oxides with large bandgaps synthesized by a chemical substitution method, *Inorg. Chem. Front.*, 2020, **7**, 4469–4476.
35 P. F. Li, C. L. Hu, F. Kong and J. G. Mao, $AAl(Te_4O_{10})$ (A = Na, Ag) and $K_2Ga_2(HTe_6O_{16})(HTeO_3)$: Three Aluminum/Gallium Tellurites with Large Birefringence and Wide Band Gap, *Inorg. Chem.*, 2023, **62**, 8494–8499.
36 D. D. Zhou, C. L. Hu, X. W. Zhang, J. G. Mao and F. Kong, Noncentrosymmetric tellurite halides created by a depolymerization strategy: toward strong SHG intensity and wide bandgap, *Chem. Sci.*, 2024, **15**, 19920–19927.

37 P. F. Li, F. Kong and J. G. Mao, $M_2IIM_3IIIF_3(Te_6F_2O_{16})$ (MII = Pb, Ba; MIII = Al, Ga): New mixed anionic tellurites with isolated Te_6 coplanar rings, *J. Solid State Chem.*, 2020, **286**, 121288.

38 P. F. Li, C. L. Hu, B. Zhang, J. G. Mao and F. Kong, From $HgGa_2(SeO_3)_4$ to $Hg_2Ga(SeO_3)_2F$: The first HgI-based selenite birefringent crystal triggered by linear groups and fluoride ions, *Chin. Chem. Lett.*, 2024, 110588, DOI: **10.1016/j.cclet.2024.110588**.

39 M. L. Liang, Y. X. Ma, C. L. Hu, F. Kong and J. G. Mao, $Ba(MoO_2F)_2(QO_3)_2$ (Q = Se, Te): Partial Fluorination of MoO_6 Octahedra Enabling Two Polar Solids with Strong and Phase Matchable SHG Response, *Chem. Mater.*, 2020, **32**, 9688–9695.

40 J. Zhou, H. Wu, H. Yu, S. Jiang, Z. Hu, J. Wang, Y. Wu and P. S. Halasyamani, $BaF_2TeF_2(OH)_2$: A UV Nonlinear Optical Fluorotellurite Material Designed by Band-Gap Engineering, *J. Am. Chem. Soc.*, 2020, **142**, 4616–4620.

41 P. F. Li, C. L. Hu, Y. F. Li, J. G. Mao and F. Kong, $Hg_4(Te_2O_5)(SO_4)$: A Giant Birefringent Sulfate Crystal Triggered by a Highly Selective Cation, *J. Am. Chem. Soc.*, 2024, **146**, 7868–7874.

42 P. F. Li, C. L. Hu, J. G. Mao and F. Kong, $Hg_2(SeO_3)(TeO_3)$: a novel tellurite–selenite birefringent crystal achieved by assembling multiple functional groups, *J. Mater. Chem. C*, 2025, **13**, 4374–4378.

43 G. M. Sheldrick, Crystal structure refinement with SHELXL, *Acta Crystallogr., Sect. C:Struct. Chem.*, 2015, **71**, 3–8.

44 O. V. Dolomanov, L. J. Bourhis, R. J. Gildea, J. A. K. Howard and H. Puschmann, OLEX2: a complete structure solution, refinement and analysis program, *J. Appl. Crystallogr.*, 2009, **42**, 339–341.

45 R. H. Blessing, An empirical correction for absorption anisotropy, *Acta Crystallogr., Sect. A:Found. Crystallogr.*, 1995, **51**, 33–38.

46 A. L. Spek, Single-crystal structure validation with the program PLATON, *J. Appl. Crystallogr.*, 2003, **36**, 7–13.

47 P. Kubelka and F. Munk, An Article on Optics of Paint Layers, *Technol. Phys.*, 1931, **12**, 259–274.

48 D. D. Zhou, C. L. Hu, J. G. Mao and F. Kong, $Ag_3In_3(SeO_3)_3(SO_4)F_4$: A Sulfate Selenite Nonlinear Optical Material with a Wide Bandgap, *Inorg. Chem.*, 2025, **64**, 19956–19960.

49 P. F. Li, X. X. Wang, C. L. Hu, J. G. Mao and F. Kong, $La_2Zn_3(SeO_3)_6$: A UV Selenite Crystal with Second-Harmonic Generation and Large Birefringence, *Inorg. Chem.*, 2025, **64**, 8856–8862.

50 X. Wang, X. Wen, Y. Yan, J. Chen, G. Yang, G. Peng and N. Ye, From $Ca_3Be(SeO_3)_4$ to $SrBe(SeO_3)_2$: two unprecedented alkaline earth metal beryllium selenites with large band gaps and enhanced birefringence, *Inorg. Chem. Front.*, 2025, **12**, 3179–3185.

51 F. Kong, T. T. He and J. G. Mao, Potassium Molybdenum Tellurite Crystals: Design, Synthesis, and Second-Order Nonlinear Optical Properties, *J. Synth. Cryst.*, 2025, **54**, 1811–1822.

52 C. Wu, X. Jiang, L. Lin, Z. Lin, Z. Huang, M. G. Humphrey and C. Zhang, $AGa_3F_6(SeO_3)_2$ (A = Rb, Cs): A New Type of Phase-Matchable Hexagonal Tungsten Oxide Material with Strong Second-Harmonic Generation Responses, *Chem. Mater.*, 2020, **32**, 6906–6915.

53 S. Shi, C. Lin, D. Zhao, M. Luo, L. Cao, G. Peng and N. Ye, Unexpected aliovalent cation substitution between two NLO materials $LiBa_3Bi_6(SeO_3)_7F_{11}$ and $Ba_3Bi_{6.5}(SeO_3)_7F_{10.5}O_{0.5}$, *Chem. Commun.*, 2021, **57**, 2982–2985.

54 J. Y. Chung, H. Jo, S. Yeon, H. R. Byun, T. S. You, J. I. Jang and K. M. Ok, $Bi_3(SeO_3)_3(Se_2O_5)F$: A Polar Bismuth Selenite Fluoride with Polyhedra of Highly Distortive Lone Pair Cations and Strong Second-Harmonic Generation Response, *Chem. Mater.*, 2020, **32**, 7318–7326.

55 C. L. Hu, Y. X. Han, Z. Fang and J. G. Mao, Zn_2BS_3Br: An Infrared Nonlinear Optical Material with Significant Dual-Property Enhancements Designed through a Template Grafting Strategy, *Chem. Mater.*, 2023, **35**, 2647–2654.

56 Y. Zheng, Q. Li, H. Wu, Z. Hu, J. Wang, Y. Wu and H. Yu, Unprecedented v-shaped $[SeO_2E]$ units stabilized in $KM[Se_2O_5]_2[SeO_2]$ (M = Al and Ga) constructed by nanoconfinement strategy, *Innovation Mater.*, 2025, 100160, DOI: **10.59717/j.xinn-mater.2025.100160**.

57 (*a*) CCDC 2500271: Experimental Crystal Structure Determination, 2025, DOI: **10.25505/fiz.icsd.cc2pxqx8**; (*b*) CCDC 2500272: Experimental Crystal Structure Determination, 2025, DOI: **10.25505/fiz.icsd.cc2pxqy9**; (*c*) CCDC 2500273: Experimental Crystal Structure Determination, 2025, DOI: **10.25505/fiz.icsd.cc2pxqzb**.